PETROLOGY

Garnet crystallization does not drive oxidation at arcs

Megan Holycross[1,2]* and Elizabeth Cottrell[2]

Arc magmas, the building blocks of continental crust, are depleted in total iron (Fe), have higher ratios of oxidized Fe to total Fe ($Fe^{3+}/\sum Fe$), and record higher oxygen fugacities (fO_2's) compared with magmas erupted at mid-ocean ridges. Garnet crystallization could explain these observations if garnet removes substantial amounts of Fe^{2+}, but not Fe^{3+}, from magma, yet this model for continental crust generation has never been tested experimentally. Analysis of garnets and melts in laboratory experiments show that the compatibilities of Fe^{2+} and Fe^{3+} in garnet are of similar magnitudes. Our results indicate that fractional crystallization of garnet-bearing cumulates will remove 20% of total Fe from primary arc basalts but negligibly alter the $Fe^{3+}/\sum Fe$ ratio and fO_2 of the melt. Garnet crystallization is unlikely to be responsible for the relatively oxidized nature of basaltic arc magmas or the Fe-depletion trend observed in continental crust.

The trace-element signatures of arc lavas mirror those of the continental crust, suggesting that subduction zone magmatism is linked to the growth of continents (*1*). Arc lavas are also oxidized relative to lavas erupted in other tectonic settings (*2*). Resolving the source of oxidation in the subduction system is then critical for understanding the evolution of continental crust and formation of ore deposits. The oxidized nature of arc magmas may arise from melting of mantle oxidized by material liberated from subducted lithosphere (*3*–*10*). Conversely (or in addition), arc magmas may oxidize in the crust as a result of magmatic differentiation (*11*, *12*). In the latter category, high-pressure fractional crystallization of garnet-bearing cumulates may act to remove more ferrous than ferric iron from melts, such that a "crustal redox filter" oxidizes arc magmas after they have separated from their mantle sources (*13*–*15*). In the "crustal redox filter" scenario, the crystallization of Fe-enriched garnet would also result in the generation of melts depleted in their total Fe contents—a common feature of calc-alkaline magmas found at continental margins. We provide direct measurements of the oxidation state of Fe in experimental garnets and melts equilibrated under controlled conditions to determine if the crystallization of garnet is compatible with the production of oxidized, Fe-depleted arc magmas that are characteristic of the continental crust.

Cumulates bearing garnet+pyroxene±rutile assemblages (i.e., garnet pyroxenites) may crystallize in magmas formed at continental arc volcanoes where the overriding crust is ≥35 km thick [e.g., (*16*–*18*)]. Previous work has suggested that low $Fe^{3+}/\sum Fe$ [$Fe^{3+}/\sum Fe$ = 0.04 to 0.08; (*15*)], Fe-enriched garnet pyroxenites are the complements to high $Fe^{3+}/\sum Fe$ [$Fe^{3+}/\sum Fe$ = 0.15 to 0.35 (*2*, *4*, *6*, *9*)], Fe-depleted arc magmas (*15*). Garnet fractionation has been proposed to be a key aspect for forming large Cu ore bodies (*19*) because porphyry copper deposits are typically associated with thick-crusted, mature arc volcanoes with oxidized magmas (*20*, *21*).

These hypotheses require that the compatibility of Fe^{2+} in garnet be much greater than the compatibility of Fe^{3+} in garnet as it crystallizes from primitive arc magmas in the crust, resulting in an increase in the $Fe^{3+}/\sum Fe$ ratio and fO_2 of the magma. However, if the compatibilities of Fe^{3+} and Fe^{2+} in garnet are similar, little fractionation of Fe species between garnet and liquid will occur during cumulate crystallization (or later remelting of cumulate phases).

Partitioning of Fe species between garnet and melt

With new laboratory measurements of Fe^{3+} and Fe^{2+} partitioning between garnet and melt, we directly evaluate the role that garnet fractionation could play in generating Fe-depleted melts with $Fe^{3+}/\sum Fe$ ratios elevated above those derived from low-pressure fractionation in the absence of garnet (as found at ridges and thin-crusted arcs). We equilibrated garnet and silicate melts from hydrous basaltic bulk compositions in 13 piston-cylinder experiments that simulated conditions in deep crustal magma chambers (T = 950° to 1230°C, P = 1.5 to 3.0 GPa). Experiment fO_2's, ranging from 0.8 logarithmic units below to 6.4 logarithmic units above the quartz-fayalite-magnetite (QFM) buffer, were set using multiple O_2-buffering approaches (*22*). Experiments (Fig. 1) cosaturated in pyrope-rich garnets with subequal almandine and grossular components, clinopyroxene (cpx) ± rutile, and quartz [see (*22*, *23*) for full details].

We measured the $Fe^{3+}/\sum Fe$ ratios of experimental garnets and silicate melts with Fe K-edge micro x-ray absorption near-edge structure (μ-XANES) spectroscopy. We calculated the concentrations of ferric and ferrous iron in both phases from measurements of glass and garnet $Fe^{3+}/\sum Fe$ ratios and FeO_T contents (i.e., all Fe present expressed as Fe^{2+}). We calculated coefficients for the partitioning of Fe^{2+} and Fe^{3+} between garnet (grt) and melt as

$$D_{Fe^{3+}}^{grt/melt} = \frac{Fe^{3+}grt}{Fe^{3+}melt} \quad (1)$$

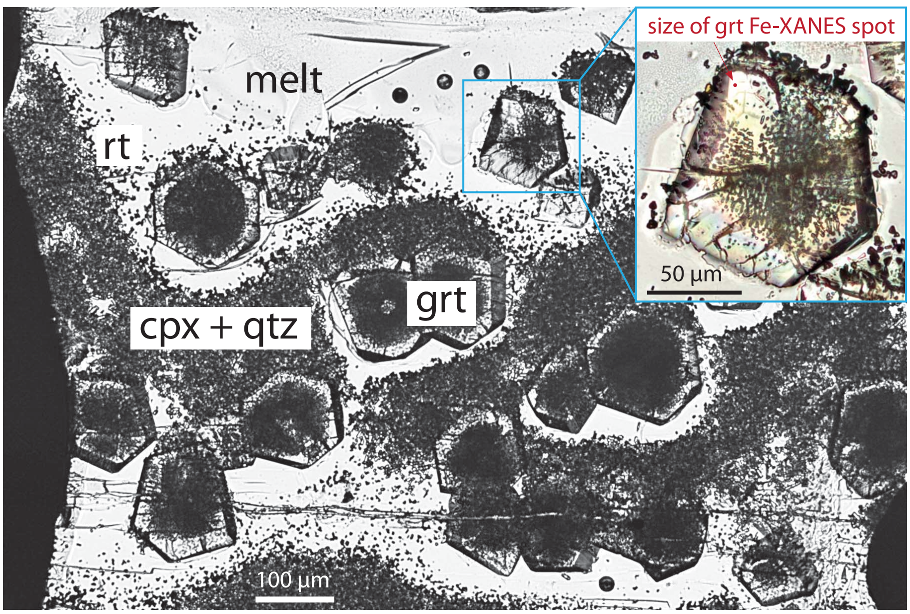

Fig. 1. Transmitted light micrograph of garnet-melt partitioning experiment. This experiment (experiment 22) contains a large fraction of silicate melt, garnet (grt), clinopyroxene (cpx), rutile (rt), and quartz (qtz). Garnet cores contain abundant mineral inclusions. Enlarged inset image shows the size of a garnet XANES spot (2 μm by 2 μm) for comparison.

[1]Cornell University, Ithaca, NY 14853, USA. [2]National Museum of Natural History, Smithsonian Institution, Washington, DC 20560, USA.
*Corresponding author. Email: holycross@cornell.edu

$$D_{Fe^{2+}}^{grt/melt} = \frac{Fe^{2+}grt}{Fe^{2+}melt} \quad (2)$$

Garnet $Fe^{3+}/\sum Fe$ ratios increase as fO_2 and temperature increase at constant pressure (fig. S8). Three experiments equilibrated at 1100°C and ΔQFM+6 show that an increase in pressure from 2.0 to 3.0 GPa decreases garnet $Fe^{3+}/\sum Fe$ ratios by 36% (relative). Garnet $Fe^{3+}/\sum Fe$ ratios are lower than melt $Fe^{3+}/\sum Fe$ ratios in all experiments; however, garnets contain 2 to 10 times more total Fe compared with melts. Consequently, the calculated partition coefficients show that Fe^{3+} is slightly incompatible to compatible in garnet (D = 0.7 to 2.4) with the greatest values of $D_{Fe^{3+}}^{grt/melt}$ measured in our coldest, most reducing experiments (Fig. 2). The decrease in $D_{Fe^{3+}}^{grt/melt}$ as fO_2 increases at constant pressure and temperature may result from a steric limit on the substitution of Fe^{3+} in pyroxenitic garnets, not unlike that observed for clinopyroxenes (*24*). The partitioning of Fe^{2+} between garnet and melt is constant across changing fO_2. Limited data from the pressure-series experiments at 1100°C and ΔQFM+6 suggest that increasing pressure decreases $D_{Fe^{3+}}^{grt/melt}$ but increases $D_{Fe^{2+}}^{grt/melt}$.

We performed multiple linear regressions to parameterize $D_{Fe^{3+}}^{grt/melt}$ and $D_{Fe^{2+}}^{grt/melt}$ in our experiments. At constant fO_2 and pressure, increasing temperature causes $D_{Fe^{2+}}^{grt/melt}$ to decrease more rapidly than $D_{Fe^{3+}}^{grt/melt}$, such that $D_{Fe^{3+}}^{grt/melt}$ and $D_{Fe^{2+}}^{grt/melt}$ converge to similar values when T > 1100°C (fig. S9). Consequently, Fe^{3+} will be minimally fractionated from Fe^{2+} in garnet-bearing melts at high temperatures and fO_2's near the QFM buffer, where the compatibilities of both iron species in garnet are similar. More substantial fractionation could occur during processing under colder ($T \leq 950$°C) and/or very oxidizing ($fO_2 \geq$ ΔQFM+4) conditions in which $D_{Fe^{2+}}^{grt/melt} \approx 10 D_{Fe^{3+}}^{grt/melt}$.

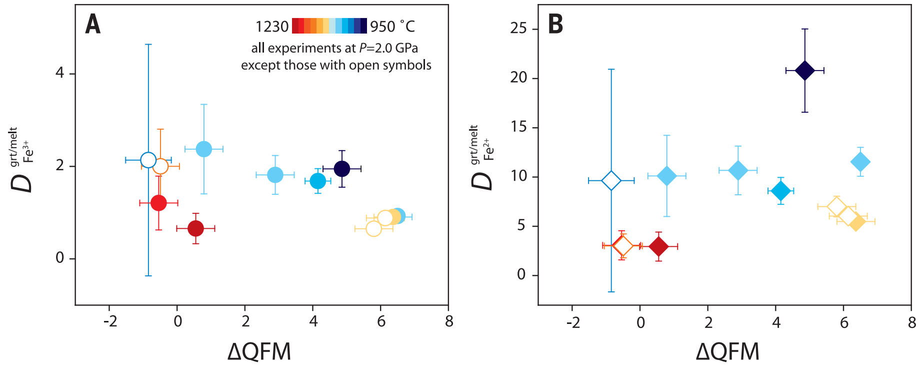

Fig. 2. Calculated partition coefficients for Fe^{2+} and Fe^{3+} in garnet. (**A**) $D_{Fe^{3+}}^{grt/melt}$ decreases as fO_2 and temperature increase. (**B**) $D_{Fe^{2+}}^{grt/melt}$ is dependent on temperature only. The total Fe content of garnet increases as temperature decreases (data S1). Data error bars are ± calculated standard errors of partition coefficients (*23*). Calculated standard errors are greatest for the most reduced experiments in which the uncertainty of the XANES calibration is large relative to the measured $Fe^{3+}/\sum Fe$ ratios of garnet.

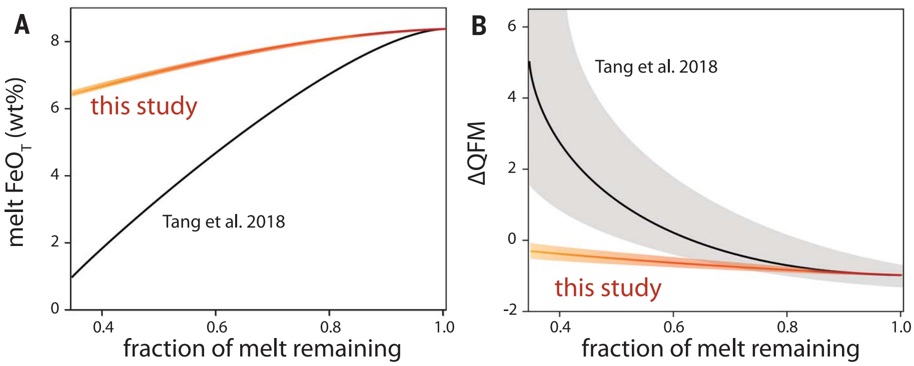

Fig. 3. Impact of garnet pyroxenite crystallization on the total Fe and fO_2 of arc magmas. We compare our model results to those of Tang *et al.* (*14*) (black curve with gray error envelope), modeled under equivalent conditions with assumed partition coefficients. The red-orange gradient of our model represents cooling from 1200°C at the onset of crystallization to 1035°C at 35% melt remaining. (**A**) The magma becomes depleted in Fe as crystallization progresses, but the trend modeled using our measured partition coefficients is moderate compared to previous work (*14*). (**B**) Our new data suggest that garnet pyroxenite fractionation will increase the fO_2 of primitive arc magmas by only 0.7 logarithmic units after >60% crystallization. Our result contrasts with the model of (*14*) that assumed $D_{Fe^{2+}}^{grt/melt} \gg D_{Fe^{3+}}^{grt/melt}$, leading to a significant increase in the $Fe^{3+}/\sum Fe$ ratio and fO_2 of residual melts during crystallization.

Deep arc magma chambers

Our data allow us to test the hypothesis that the fractionation of garnet at high pressures in the lower crust can generate Fe-depleted magmas with elevated $Fe^{3+}/\sum Fe$ ratios and high fO_2's (*14*, *15*). Previous work (*14*) suggested that the fractionation of a pyroxenite assemblage with 30 modal % garnet from a hydrous primitive magma can remove up to 60% of the Fe from the melt while increasing its fO_2 by as much as six logarithmic units. In the absence of measured ferrous-ferric garnet–melt partition coefficients, the model of Tang *et al.* (*14*) assumed perfect incompatibility of Fe^{3+} in garnet (i.e., $D_{Fe^{3+}}^{grt/melt} = 0$), and $D_{Fe^{2+}}^{grt/melt}$ was described as "significantly >1." We adopt a similar modeling approach to evaluate how our new calculated values for $D_{Fe^{3+}}^{grt/melt}$ and $D_{Fe^{2+}}^{grt/melt}$ affect this finding.

Our modeled fractionation of a cumulate with 70 modal % cpx and 30 modal % garnet begins at fO_2 = ΔQFM – 1 in a hydrous basaltic magma with $Fe^{3+}/\sum Fe$ = 0.09 (Fig. 3). We chose model conditions to facilitate direct comparison with the results of Tang *et al.* (*14*). Both ferrous and ferric iron are compatible in garnet at these conditions, but the difference between their partition coefficients is minimal ($D_{Fe^{2+}}^{grt/melt} = 2.1$; $D_{Fe^{3+}}^{grt/melt} = 1.4$; this study). We applied $D_{Fe^{3+}}^{cpx/melt}$ between 0.3 and 0.8 (*25*, *26*), represented by the width of the red-orange envelope around the modeled value (solid line) of $D_{Fe^{3+}}^{cpx/melt} = 0.6$ in Fig. 3. Ferrous iron and Mg occupy the same sites in cpx and garnet, so we tie the partitioning of Fe^{2+} to Mg in both phases using an Fe-Mg exchange coefficient, K_D Fe/Mg. We modeled the composition of the melt until ~65% fractional crystallization of garnet pyroxenite [i.e., previously published estimates of the proportion of mafic cumulates generated during arc magma differentiation in the lower crust (*27*)]. Because the physical mechanism for crystallization is likely to be cooling, we varied temperature and pressure over the fractional crystallization interval in our model beginning at 1200°C, 2.0 GPa to 1035°C, 1.3 GPa at a residual melt fraction of 0.35. Coefficients for the partitioning of ferric iron between garnet and melt and our K_D^{grt} Fe/Mg values were recalculated at each crystallization step. We assumed clinopyroxene-melt partition coefficients to be insensitive to changing pressure and temperature, and K_D^{cpx}

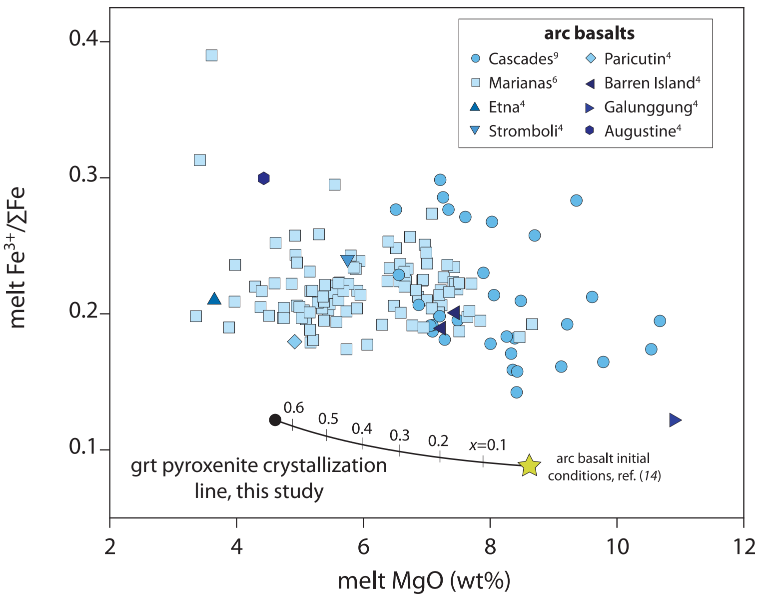

Fig. 4. Comparison between $Fe^{3+}/\sum Fe$ ratios of modeled arc magmas and measured $Fe^{3+}/\sum Fe$ ratios of arc basalts. The modeled $Fe^{3+}/\sum Fe$ ratios of primitive arc basalts that fractionate garnet pyroxenites (black line) do not approach the measured $Fe^{3+}/\sum Fe$ ratios of arc basalts (blue data points). The black line shows the $Fe^{3+}/\sum Fe$ ratio and MgO content of the residual melt modeled in Fig. 3 using garnet-melt partition coefficients for Fe species measured in this study. Crystal fractionation intervals (x) are indicated for 0.1 steps on the black line. Model initial conditions are the same as in Tang *et al*. (*14*).

Fe/Mg was set at 0.25 (*25*, *26*). Additional assumptions, parameters, and other details can be found in (*23*).

The compatibility of ferrous iron in both cpx and garnet, and ferric iron in garnet, leads to a decrease in melt FeO_T as crystallization progresses in our model (Fig. 3A). However, the degree of Fe depletion in the melt is moderate (~20%). An extreme Fe-depletion trend [≥60%, e.g., (*14*)] can only be produced through the input of unrealistically high Fe-Mg exchange coefficients (>7× measured values at relevant conditions), which results in bulk cumulate compositions with extremely low Mg numbers (Mg number of the first cumulate = 0.07; fig. S12). Our model reproduces the Mg numbers [0.43 to 0.89 (*27*)] and garnet compositions of natural pyroxenite xenoliths (fig. S10) (*23*). Pyroxenitic garnets contain subequal Fe and Mg components and only become almandine-rich during crystallization at low temperatures. Our measurements and the literature data show that the compatibility of Fe^{2+} is greater than that of Fe^{3+} in garnet [and is likely greater in cpx (*25*, *26*)], but the partition coefficients for both species in each phase are of similar magnitudes at the conditions relevant for cumulate fractionation in primitive arc magmas. Consequently, the crystallization of garnet pyroxenites, modeled using our measured partition coefficients, will only increase the $Fe^{3+}/\sum Fe$ ratio of the magma by 0.04, corresponding to a 0.8 logarithmic unit increase in the fO_2 of the residual melt after 65% fractional crystallization (Fig. 3B). The $Fe^{3+}/\sum Fe$ ratio of the residual melt does not approach the measured $Fe^{3+}/\sum Fe$ ratios of olivine-hosted arc melt inclusions and submarine glasses (*2*, *4*, *6*, *9*) over this crystallization interval (Fig. 4). The arc basalt oxidation trends of (*14*) can only be achieved if Fe^{2+} is assumed to be outstandingly compatible in garnet and cpx. Even if Fe^{3+} is modeled as perfectly incompatible in garnet, the $Fe^{3+}/\sum Fe$ ratio of the residual melt does not increase by more than 0.06, mirroring the olivine fractionation trend observed in mid-ocean ridge basalt (*23*, *28*).

Garnet crystallization does not drive oxidation at arcs

Fractionation of garnet + cpx + rutile residues has been invoked as an essential process to "auto-oxidize" the magmas associated with large copper porphyries (*19*) and to lower the Nb/Ta ratios of arc magmas generally (*29*). Our finding does not question that formation of garnet pyroxenites can be an important part of arc petrogenesis (*16*–*18*, *30*); however, it cannot "auto-oxidize" nor lower the Nb/Ta ratios of magmas. Measured rutile-melt partition coefficients demonstrate that the fractionation of rutile-bearing residues cannot explain the Nb/Ta ratios of continental crust (*31*), and it is clear from the results of this study that the crystallization of garnet pyroxenites from basaltic magmas cannot be responsible for the elevated $Fe^{3+}/\sum Fe$ ratios and high fO_2's of arc magmas and Cu porphyries, which must be produced by a different process. Our results also indicate that the Fe-depleted calc-alkaline differentiation trend cannot be attributed solely to garnet crystallization in the base of thick-crusted arcs.

REFERENCES AND NOTES

1. J. B. Gill, *Orogenic Andesites and Plate Tectonics* (Springer, 1981).
2. E. Cottrell *et al*., in *Magma Redox Geochemistry*, R. Morretti, D. R. Neuville, Eds. (Wiley, 2021), pp. 33–61.
3. B. J. Wood, L. T. Bryndzia, K. E. Johnson, *Science* **248**, 337–345 (1990).
4. K. A. Kelley, E. Cottrell, *Science* **325**, 605–607 (2009).
5. K. A. Evans, A. G. Tomkins, *Earth Planet. Sci. Lett.* **308**, 401–409 (2011).
6. M. N. Brounce, K. A. Kelley, E. Cottrell, *J. Petrol.* **55**, 2513–2536 (2014).
7. F. Gaillard, B. Scaillet, M. Pichavant, G. Iacono-Marziano, *Chem. Geol.* **418**, 217–233 (2015).
8. B. Debret, D. A. Sverjensky, *Sci. Rep.* **7**, 10351 (2017).
9. M. J. Muth, P. J. Wallace, *Geology* **49**, 1177–1181 (2021).
10. J. J. Ague *et al*., *Nat. Geosci.* **15**, 320–326 (2022).
11. C. T. Aeolus Lee, W. P. Leeman, D. Canil, Z. X. A. Li, *J. Petrol.* **46**, 2313–2336 (2005).
12. C. T. A. Lee *et al*., *Science* **336**, 64–68 (2012).
13. E. J. Chin, K. Shimizu, G. M. Bybee, M. E. Erdman, *Earth Planet. Sci. Lett.* **482**, 277–287 (2018).
14. M. Tang, M. Erdman, G. Eldridge, C. A. Lee, *Sci. Adv.* **4**, eaar4444 (2018).
15. M. Tang, C. T. A. Lee, G. Costin, H. E. Höfer, *Earth Planet. Sci. Lett.* **528**, 115827 (2019).
16. O. Müntener, P. B. Kelemen, T. L. Grove, *Contrib. Mineral. Petrol.* **141**, 643–658 (2001).
17. O. Jagoutz, O. Müntener, M. W. Schmidt, J. P. Burg, *Earth Planet. Sci. Lett.* **303**, 25–36 (2011).
18. O. Jagoutz, P. B. Kelemen, *Annu. Rev. Earth Planet. Sci.* **43**, 363–404 (2015).
19. C. T. A. Lee, M. Tang, *Earth Planet. Sci. Lett.* **529**, 115868 (2020).
20. R. H. Sillitoe, *Econ. Geol.* **105**, 3–41 (2010).
21. J. P. Richards, *Ore Geol. Rev.* **40**, 1–26 (2011).
22. M. Holycross, E. Cottrell, *Contrib. Mineral. Petrol.* **177**, 21 (2022).
23. Materials and methods are available as supplementary materials.
24. M. C. McCanta, M. D. Dyar, M. J. Rutherford, J. S. Delaney, *Am. Mineral.* **89**, 1685–1693 (2004).
25. F. A. Davis, E. Cottrell, *Contrib. Mineral. Petrol.* **176**, 67 (2021).
26. A. Rudra, M. M. Hirschmann, *Geochim. Cosmochim. Acta* **328**, 258–279 (2022).
27. C. T. A. Lee, in *Treatise on Geochemistry*, H. D. Holland, K. K. Turekian, Eds. (Elsevier, ed. 2, 2014), pp. 423-456.
28. E. Cottrell, K. A. Kelley, *Earth Planet. Sci. Lett.* **305**, 270–282 (2011).
29. M. Tang *et al*., *Nat. Commun.* **10**, 235 (2019).
30. P. Ulmer, R. Kaegi, O. Müntener, *J. Petrol.* **59**, 11–58 (2018).
31. M. Holycross, E. Cottrell, *Am. Mineral.* **105**, 244–254 (2020).

ACKNOWLEDGMENTS

Thanks to A. Woodland for garnet reference materials; F. Davis, M. Muth, M. Brounce, and J. Ague for helpful discussion; T. Gooding, T. Rose, E. Gazel, J. B. Balta, J. Thomas, and G. Macpherson for laboratory help; and A. Lanzirotti, M. Newville, K. Kelley, J. Andrys, and R. Tappero for beamline assistance. We are grateful to L. Hale and C. Brown for assistance with reference materials borrowed from the National Rock Collection at the Smithsonian. We thank two anonymous reviewers for detailed and constructive comments that improved the manuscript. **Funding:** National Science Foundation grant EAR 1855208 (M.H.), Smithsonian Scholarly Studies and the Lyda Hill Foundation (E.C.), and NMNH Peter Buck Fellowship (M.H.). This research used resources of the National Synchrotron Light Source II, a US Department of Energy (DOE) Office of Science User Facility operated for the DOE Office of Science by Brookhaven National Laboratory under contract no. DE-SC0012704, and resources of the Advanced Photon Source, a US DOE Office of Science user facility operated for the DOE Office of Science by Argonne National Laboratory under contract no. DE-AC02-06CH11357. **Author contributions:** Conceptualization, Methodology, Investigation, Visualization, and Funding Acquisition: M.H. and E.C.. First Draft: M.H.. Review and Editing: M.H. and E.C. **Competing interests:** The authors declare that they have no competing interests. **Data and materials availability:** All data are available in the manuscript or the supplementary materials.

SUPPLEMENTARY MATERIALS

science.org/doi/10.1126/science.ade3418
Materials and Methods
Supplementary Text
Figs. S1 to S13
Tables S1 and S2
References (*32–69*)
Data S1 and S2

Submitted 10 August 2022; accepted 30 March 2023
10.1126/science.ade3418

Garnet crystallization does not drive oxidation at arcs

Megan Holycross and Elizabeth Cottrell

Science, **380** (6644), .
DOI: 10.1126/science.ade3418

Editor's summary
The formation of garnet-bearing cumulates is one leading candidate to explain the chemistry of oceanic arc lavas, which are ultimately responsible for building continents. Holycross and Cottrell tested this hypothesis by running a series of experiments to determine how garnet formation changes the amount and speciation of iron. They found that garnet does not have a large impact and is unlikely to be the sole cause of the oxidation of arc lavas. The observed chemistry requires a different explanation. —Brent Grocholski